



ELSEVIER

Tectonophysics 352 (2002) 317–333

TECTONOPHYSICS

www.elsevier.com/locate/tecto

On the role of subducting oceanic plateaus in the development of shallow flat subduction

Jeroen van Hunen*, Arie P. van den Berg, Nico J. Vlaar

Department of Theoretical Geophysics, Institute of Earth Sciences, University of Utrecht, P.O. Box 80 021, 3508 TA Utrecht, The Netherlands

Received 6 June 2001; accepted 2 May 2002

Abstract

Oceanic plateaus, aseismic ridges or seamount chains all have a thickened crust and their subduction has been proposed as a possible mechanism to explain the occurrence of flat subduction and related absence of arc magmatism below Peru, Central Chile and at the Nankai Trough (Japan). Their extra compositional buoyancy could prohibit the slab from sinking into the mantle. With a numerical thermochemical convection model, we simulated the subduction of an oceanic lithosphere that contains an oceanic crustal plateau of 18-km thickness. With a systematic variation, we examined the required physical parameters to obtain shallow flat subduction. Metastability of the basaltic crust in the eclogite stability field is of crucial importance for the slab to remain buoyant throughout the subduction process. In a 44-Ma-old subducting plate, basalt must be able to survive a temperature of 600–700 °C to keep the plate buoyant sufficiently long to cause a flat-slab segment. We found that the maximum yield stress in the slab must be limited to about 600 MPa to allow for the necessary bending to the horizontal. Young slabs show flat subduction for larger parameter ranges than old slabs, since they are less gravitationally unstable and show less resistance against bending. Hydrous weakening of the mantle wedge area and lowermost continent are required to allow for the necessary deformation of a change in subduction style from steep to flat. The maximum flat slab extent is about 300 km, which is sufficient to explain the observed shallow flat subduction near the Nankai Trough (Japan). However, additional mechanisms, such as active overthrusting by an overriding continental plate, need to be invoked to explain the flat-slab segments up to 500 km long below Peru and Central Chile.

© 2002 Elsevier Science B.V. All rights reserved.

Keywords: Flat subduction; Buoyancy; Rheology; Oceanic plateaus; Metamorphism; Kinetics

1. Introduction

The subduction of regions of oceanic lithosphere with overthickened crust (aseismic ridges, oceanic plateaus or seamount chains) seems to coincide spa-

tially and temporally with the absence of arc volcanism (McGeary et al., 1985). In some of these cases, the slab dips more shallow or even horizontal at a depth of approximately 100 km. For example, gaps in recent active volcanism at low-angle subduction below Peru, Central Chile and at the Nankai trough near Japan seem to be related to the subduction of the Nazca Ridge, Juan Fernandez seamount chain and Palau–Kyushu Ridge, respectively (Cross and Pilger,

* Corresponding author. Present address: Department of Physics, University of Colorado, Boulder, CO 80309, USA.

E-mail address: hunen@anquetil.colorado.edu (J. van Hunen).

1982; McGeary et al., 1985). For these areas, a flat slab is observed at 200 km (Nankai) and 700 km (Peru and Chile) from the trench (Sacks, 1983; McGeary et al., 1985). In fact, flat subduction occurs at about 10% of the modern convergent margins, and most of these regions correlate with a subducting plateau or aseismic ridge (Gutscher et al., 2000). Under such circumstances, absence of arc volcanism is explained by the disappearance of the mantle wedge with decreasing dip angle: contact of the hydrated subducted crust with the hot asthenosphere is absent, which stops partial melting and associated volcanism. Flat subduction of an even larger scale has been proposed to explain the formation of the Rocky Mountains during the Laramide orogeny (Dickinson and Snyder, 1978; Bird, 1988), although for this event no evidence of subducting oceanic plateaus is available.

The correlation between the subduction of oceanic plateaus and the occurrence of flat subduction suggests these plateaus to be anomalously buoyant. The thicker crust is underlain by a proportionally thicker harzburgite layer. During subduction, the gabbroic or basaltic crust transforms into eclogite. Eclogite and harzburgite have compositional buoyancies of opposite sign relative to undepleted mantle material (Irfune and Ringwood, 1993) that approximately cancel each other within an oceanic lithosphere. Only before eclogitisation, the subducting slab has its compositional buoyancy dependent on the crustal thickness. If the eclogite formation would occur under near-equilibrium conditions, shallower than 70–80-km depth (Kirby et al., 1996a), slabs would lose their compositional buoyancy at this shallow depth, regardless of their crustal thickness. Only a kinetically hindered reaction from basalt to eclogite would cause the slab to preserve (some of) its compositional buoyancy to greater depth. Therefore, the hypothesis that buoyant plateaus cause flat subduction implicitly assumes a significant kinetic delay of eclogitisation of the crust.

The kinetics of the basalt-to-eclogite transition has been subject of research for several decades. Ahrens and Schubert (1975) report no significant reaction rates under completely dry conditions, but geologically fast reaction rates with the addition of water. More recent experiments (e.g. Holland, 1980 vs. Hacker et al., 1993) did not lead to consensus about the metamorphic reaction rates in the oceanic crust under subduction conditions (Hacker, 1996). Geo-

logical observations (pT paths) suggest a wide range of possible reaction rates (Hacker, 1996; Austrheim, 1998): complete transformation at 450 °C and incomplete transformation at 800 °C are both recorded. The degree of hydration is probably at least as significant as the ambient temperature and pressure and dry rocks can remain metastable for a long time (Rubie, 1990; Austrheim, 1998). Furthermore, deformation both enhances the reaction rates and facilitates the access of fluids (Saunders et al., 1996). Complete and incomplete reaction to eclogite have also been suggested on the basis of seismological studies (Gubbins and Snieder, 1991; Kirby et al., 1996a; Abers, 2000).

Increased buoyancy of the overthickened crust is not the only proposed mechanism to explain shallow flat subduction. Nonhydrostatic pressure forces (Jischke, 1975) or a slab suction force (Stevenson and Turner, 1977; Tovish et al., 1978) and active overthrusting of the overriding continent (lithospheric doubling) (Vlaar, 1983; van Hunen et al., 2000) are proposed as alternative mechanisms. In fact, the largest flat-slab segments (Central Chile and Peru) occur below the fastest overriding plate motion (Jarrard, 1986). This suggests that active overthrusting plays a significant role in the creation of a horizontally subducting slab. However, the striking correlation between the subducting plateau locations and the sites of shallow flat subduction suggests an important influence of these plateaus on the subduction process.

Although several mechanisms have been proposed for the absence of arc volcanism above subducting plateaus, for the preservations of the compositional buoyancy of the plateaus and for the dynamics of the slab flattening, quantitative models are rare or absent. In this paper, we determine the viability and importance of shallow flat slab development in the presence of a subducting ‘buoyant plateau’ with a numerical model.

2. Model description

2.1. Governing equations and rheology description

To study the dynamics of a thickened crust within a subducting oceanic lithosphere, we have developed a two-dimensional numerical model based on finite element methods. We adopt the extended Boussinesq

approximation (EBA) (Steinbach et al., 1989; Ita and King, 1994) and use a nondimensionalization scheme as in van den Berg et al. (1993). In nondimensional form, the governing equations are:

$$\partial_j u_j = 0 \tag{1}$$

$$\begin{aligned} \partial_j(\eta \dot{\epsilon}_{ij}) - \partial_i \Delta P \\ = \left(RaT - \sum_k Rb_k \Gamma_k + RcC \right) \delta_{iz} \end{aligned} \tag{2}$$

$$\begin{aligned} \frac{\partial T}{\partial t} + u_j \partial_j T - Di(T + T_0)w - \sum_k \gamma_k \frac{Rb_k}{Ra} Di \\ (T + T_0) \frac{d\Gamma_k}{dt} - \partial_j \partial_j T = \frac{Di}{Ra} \Phi + H \end{aligned} \tag{3}$$

$$\frac{\partial C}{\partial t} + u_j \partial_j C = 0 \tag{4}$$

Eqs. (1)–(4) describe conservation of mass, momentum, energy, and composition, respectively. Symbols are explained in Table 1. The model distinguishes between crustal and mantle material, where the latter is subdivided into depleted harzburgite and undepleted peridotite. We use a composite rheology of several deformation mechanisms, for crust and mantle material separately. The effective viscosity is defined as in van den Berg et al. (1993):

$$\eta_{k,\text{eff}} = \left(\sum_m (\eta_{k,m})^{-1} \right)^{-1} \tag{5}$$

where k refers to the material and m to the deformation mechanism. Each $\eta_{k,m}$ defines the viscosity corresponding to a single deformation mechanism in a given material. For two deformation mechanisms, diffusion creep and dislocation creep, an Arrhenius flow law is used:

$$\eta_m = A_m^{-1/n_m} \dot{\epsilon}^{(1-n_m)/n_m} \exp\left(\frac{E_m^* + pV_m^*}{n_m RT}\right) \tag{6}$$

where the material subscript k is omitted for clarity. Diffusion creep is not considered for crustal material.

We used a material-independent stress limiting rheology with a yield viscosity

$$\eta_y = \tau_y \dot{\epsilon}_y^{-1/n_y} \dot{\epsilon}^{1/n_y-1} \tag{7}$$

as an additional deformation mechanism in Eq. (5) to limit the strength of the material to approximately the yield stress τ_y . The powerlaw index n_y defines the ‘brittleness’ of the stress limited material: the ‘Newtonian’ limit is $n_y = 1$ where η_y is independent of stress or strainrate and a ‘viscosity limiter’ would be a more appropriate term, while the ‘brittle’ limit of a very large n_y refers to a maximum stress, regardless of the strainrate. For intermediate values, the stress limiter behaves like a powerlaw creep mechanism. We applied the value $n_y = 5$ in all models. This stress limiter effectively replaces other deformation mechanisms, such as the Peierl mechanism (Kameyama et al., 1999), which is not implemented here.

The mantle flow laws used apply to dry material. However, the volume above a subducting slab (i.e. the mantle wedge and lowermost continent) is hydrated (Karato, submitted for publication), most likely by continuous dehydration of the subducting slab and dry flow laws would overestimate the local strength (Mei and Kohlstedt, 2000a,b; Karato and Jung, submitted for publication). Therefore, in some model calculations, we included in this area a simple parameterization of rheological weakening, relative to the dry mantle strength, represented by a multiplication constant. Similarly, Billen and Gurnis (2001) used a weak mantle wedge to explain observed topography, gravity and geoid signals. Tables 2 and 3 describe the set of used rheological parameters.

2.2. Model setup

We used a 2-D 2000-km deep Cartesian box to model the subduction process. Horizontally, the model is subdivided into a subducting oceanic part on the left and a static continental part on the right, as illustrated in Fig. 1. The oceanic lithosphere ranges from a midocean ridge (MOR) in the upperleft corner of the model box to a trench to the right of which a 2200-km wide continent is positioned.

The large-scale driving mechanism of most subduction processes is dominated by the slab pull. This, however, cannot result in flat subduction, since slab

Table 1
Notations

Symbol	Meaning	Value used	Dimension
$A_{k,m}$	Preexponential flow law parameter	–	$\text{Pa}^{-n} \text{s}^{-1}$
A_{kin}	Kinetic preexponent	10^{-6}	$\text{K}^{-1} \text{s}^{-1}$
C	Composition parameter	–	–
c_p	Specific heat	1250	$\text{J kg}^{-1} \text{K}^{-1}$
Di	Dissipation number = $\alpha gh/c_p$	0.47	–
$E_{k,m}^*$	Activation energy	–	J mol^{-1}
E_{kin}^*	Kinetic activation energy	–	J mol^{-1}
H	Nondimensional radiogenic heat production	–	–
k	Material index	–	–
m	Deformation mechanism index	–	–
$n_{k,m}$	Viscosity stress exponent	–	–
n_y	Yield stress exponent	5	–
Q_L	Latent heat release across a phase transition	–	J kg^{-1}
R	Gas constant	8.3143	$\text{J K}^{-1} \text{m}^{-3}$
Ra	Thermal Rayleigh number $\rho \alpha \Delta T h^3 / \eta \kappa$	1.8×10^7	–
Rb	Phase Rayleigh number $\delta \rho g h^3 / \eta \kappa$	2.4×10^7	–
Rc	Compositional Rayleigh number $\Delta \rho_c g h^3 / \eta \kappa$	2.4×10^7	–
T	Nondimensional temperature	–	–
T_0	Nondimensional surface temperature	$273/\Delta T$	–
ΔG	Gibbs free energy between basalt and eclogite	–	J mol^{-1}
ΔP	Nondimensional hydrodynamic pressure	–	–
ΔT	Temperature contrast across model domain	2300	K
t	Nondimensional time	–	–
t_{tr}	Transition time for the eclogitisation reaction	10	Ma
\mathbf{u}	Nondimensional velocity $\mathbf{u}=(v, w)^T$	–	–
$V_{k,m}^*$	Activation volume	–	$\text{m}^3 \text{mol}^{-1}$
Y	Growth function of the eclogitisation reaction	–	–
α	Thermal expansion coefficient	3×10^{-5}	K^{-1}
Γ_k	Phase functions for all k mantle phase transitions	–	–
γ_{400}	Clapeyron slope 400-km phase transition	3	MPa K^{-1}
γ_{670}	Clapeyron slope 670-km phase transition	–2.5	MPa K^{-1}
ΔG	Gibbs free energy difference between reaction products	–	J mol^{-1}
$\Delta \rho_c$	Compositional density relative to mantle material		
	Basalt	–400	kg m^{-3}
	Eclogite	+200	kg m^{-3}
	Harzburgite	–77	kg m^{-3}
δT	Temperature increase due to latent heat release	–	K
δz	Phase transition deflection	–	m
$\delta \rho_{400}$	Density difference across the 400-km phase transition	273	kg m^{-3}
$\delta \rho_{670}$	Density difference across the 670-km phase transition	342	kg m^{-3}
$\dot{\epsilon}_{ij}$	$\dot{\epsilon}_{ij} = \partial_j u_i + \partial_i u_j$ = strainrate tensor	–	s^{-1}
$\dot{\epsilon}$	Second invariant of the strainrate	–	s^{-1}
$\dot{\epsilon}_y$	Reference strainrate in yield strength determination	10^{-15}	s^{-1}
η	Nondimensional viscosity	–	–
Θ	Nondimensional eclogitisation rate	–	–
Φ	Nondimensional viscous dissipation	–	–
ρ	Mantle density	3416	kg m^{-3}
τ_y	Yield stress	–	Pa
τ_{ij}	Deviatoric stress tensor	–	Pa
τ	Second invariant of the stress tensor τ_{ij}	–	Pa
τ_y	Yield stress for strainrate $\dot{\epsilon}_y$	–	Pa

Table 2
Rheological parameters

Symbol	Meaning	Value used	Dimension
$A_{k,m}$	Preexponential flow law parameter		
	Crustal dislocation creep value	7.4×10^{-39}	$\text{Pa}^{-n} \text{s}^{-1}$
	Reference mantle diffusion creep value ^a	3.04×10^{-11}	$\text{Pa}^{-n} \text{s}^{-1}$
$E_{k,m}^*$	Reference mantle dislocation creep value ^a	3.84×10^{-16}	$\text{Pa}^{-n} \text{s}^{-1}$
	Activation energy		
	Crustal dislocation creep value	0	J mol^{-1}
$n_{k,m}$	Reference mantle diffusion creep value ^a	300×10^3	J mol^{-1}
	Reference mantle dislocation creep value ^a	540×10^3	J mol^{-1}
	Viscosity stress exponent		
n_y	Crustal dislocation creep value ^b	3.4	–
	Reference mantle diffusion creep value ^a	1.0	–
	Reference mantle dislocation creep value ^a	3.5	–
$V_{k,m}^*$	Yield stress exponent	5	–
	Activation volume		
	Crustal dislocation creep value	0	$\text{m}^3 \text{mol}^{-1}$
$\dot{\epsilon}_y$	Reference mantle diffusion creep value	4.5×10^{-6}	$\text{m}^3 \text{mol}^{-1}$
	Reference mantle dislocation creep value ^c	14×10^{-6}	$\text{m}^3 \text{mol}^{-1}$
	Reference 'yield strainrate'	10^{-15}	s^{-1}

^a Karato and Wu (1993).

^b Shelton and Tullis (1981).

^c Karato and Rubie (1997).

pull acts vertically. If an oceanic plateau is able to support a flat slab, this is a direct indication that its buoyancy force exceeds the slab pull. This implies

Table 3
Definition of the model calculations

Model	Oceanic plateau present	Slab age (Ma)	T_{tr} (°C)	E_{kin}^* (kJ/mol)	τ_y (MPa)	Relative mantle wedge weakening
REFp	yes	44	700	214	200	0.1
REFnp	no	44	700	214	200	0.1
KIN1	yes	44	400	146	200	0.1
KIN2	yes	44	500	169	200	0.1
KIN3	yes	44	600	192	200	0.1
KIN4	yes	44	800	238	200	0.1
YLD1	yes	44	700	214	100	0.1
YLD2	yes	44	700	214	300	0.1
YLD3	yes	44	700	214	400	0.1
YLD4	yes	44	700	214	500	0.1
YLD5	yes	44	700	214	600	0.1
YLD6	yes	44	700	214	700	0.1
YLD7	yes	44	700	214	800	0.1
YLD8	yes	44	700	214	900	0.1
YLD9	yes	44	700	214	1000	0.1
AGE1	yes	20	700	214	200	0.1
AGE2	yes	32	700	214	200	0.1
AGE3	yes	56	700	214	200	0.1
WMW1	yes	44	700	214	200	1.0
WMW2	yes	44	700	214	200	0.05

that the plateau would not subduct at all, if it was not part of a much larger and rather rigid oceanic plate, which determines the subduction velocity. To simulate these conditions in our models, we impose a constant trenchward velocity on the plate to be subducted. A 5-cm/year subduction velocity is imposed through a trenchward oceanic surface velocity boundary condition in combination with a nonmoving continent. The converging plates are decoupled by a free-slip fault extending up to 100-km depth and the rather weak interface of the subducting oceanic crust. The model does not contain a forebulge, and the dip angle of the curved fault increases from zero (horizontal) to about 23° at 100-km depth. The distance from MOR to trench and the subduction velocity determine the age of the slab near the trench. This age, as well as the prescribed subducting plate velocity and the distance from MOR to trench, are kept constant throughout each model calculation.

Thermal initial and boundary conditions, as well as the radiogenic heat production, are similar to a previous model (van Hunen et al., 2000). The initial geotherm is defined by an adiabat for the oceanic subsurface and a steady state, 60 mW m⁻² surface continental heatflow geotherm with radiogenic heat production distribution from Chapman (1986). Ther-

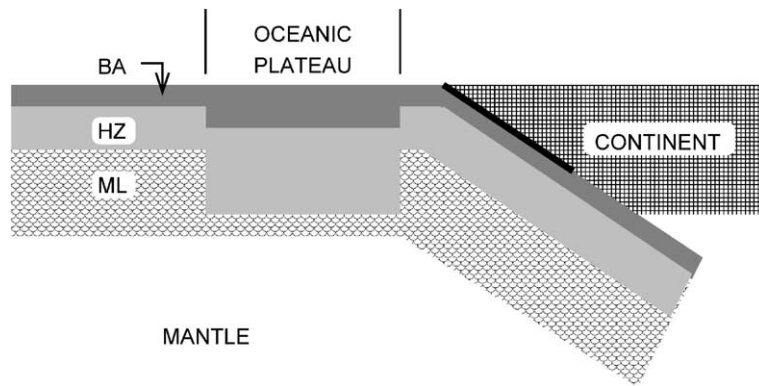


Fig. 1. Schematic diagram of the numerical model setup. A layered oceanic lithosphere contains an oceanic plateau, which is subducted below a continent with 5 cm/year. BA = basalt, HZ = harzburgite and ML = mantle lithosphere. The solid line represents a free-slip fault to decouple the plates.

mal boundary conditions are a mantle adiabat (potential temperature $T_p = 1300$ °C) at the left-hand side and bottom boundary, $T = 0$ °C at the surface and a continental geotherm on the right hand side boundary. A starting situation of ‘unperturbed’ Benioff subduction was created by an initial 16-Ma-lasting oceanic subduction process with 5 cm/year. During this initial stage, the tip of the slab reaches the transition zone. We define model time $t = 0$ at the end of this initial stage. The oceanic lithosphere is stratified with a 7-km thick crust and an 18-km thick harzburgite layer on top of undepleted peridotite. If applied, a 400-km wide oceanic plateau is positioned in front of the trench at $t = 0$, where the crustal and harzburgitic layers are 18 and 46.2 km thick, respectively. The major mantle phase transitions at 400- and 670-km depth are included using a 20-km wide harmonic parameterization of the phase functions Γ_k in Eqs. (2) and (3). Relative compositional densities and density changes across the mantle phase transitions are listed in Table 1. Both buoyancy effects as a result of phase boundary deflection and latent heat production/consumption (van Hunen et al., 2001) terms are taken into account. We did not include olivine metastability, since, regarding the low age of the slabs, it is unlikely to be significant (Kirby et al., 1996b; Schmeling et al., 1999). For a more elaborate description of the implementation, effects and applied parameters of the mantle phase transitions, we refer to van Hunen et al. (2001).

2.3. Eclogitisation and reaction kinetics

Basalt or gabbro transforms into eclogite during the subduction process, thereby neutralizing the compositional buoyancy of the subducting slab (Table 1). We implemented crustal metamorphism and included the possibility of kinetic hindrance of the metamorphic reaction. Detailed descriptions of phase change kinetics are given in Kirby et al. (1996b), Riedel and Karato (1996) and Däßler et al. (1996), applied to the well-studied and well-constrained olivine-to-spinel transition. For varying pressure and temperature conditions, the reaction rate $\Theta = d\Gamma/dt$ is a function of time-dependent nucleation and growth functions I and Y (Kirkpatrick, 1976; Däßler et al., 1996). Here, we approximate this rate with a simpler description for time-independent nucleation and growth functions, also known as the Avrami equation:

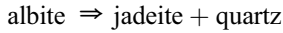
$$\Gamma = 1 - \exp(-a^4 I Y^3 t^4) \quad (8)$$

A general Arrhenius formulation of the growth function Y is given by (Däßler et al., 1996):

$$Y \sim T \exp\left(\frac{-E_{\text{kin}}^*}{RT}\right) \left[1 - \exp\left(\frac{\Delta G}{RT}\right)\right] \quad (9)$$

where E_{kin}^* is the activation energy for growth and ΔG the Gibbs free energy change between basalt and eclogite. The basalt-to-eclogite kinetic properties are

less well known than those of the olivine-to-spinel transition, partly because crustal materials are less extensively studied than olivine, and partly because the role of hydration is less certain. Therefore, we decided to use the approach from [Giunchi and Ricard \(1999\)](#). First, they describe the kinetics of crustal metamorphism in a simplified system with the reaction



for which the necessary parameters (Gibbs free energy difference, Clapeyron slope, etc.) are relatively well known ([Putnis, 1992](#)). Second, they assume a nucleation function I with a p - T dependence of the same form as the growth function Y . We believe that this is a justified approximation because of the large uncertainties in the crustal kinetic parameters. Now Eq. (8) reduces to:

$$\Gamma = 1 - \exp(-A_{\text{kin}} Y t^4) \quad (10)$$

and the reaction rate Θ closely resembles the function

$$\Theta = 4A_{\text{kin}} Y ((\Gamma(1 - \Gamma))^{3/4} + \epsilon) \quad (11)$$

which is symmetric about $\Gamma=0.5$, and where $\epsilon=10^{-3}$ is a small constant to start the reaction. Despite the simplifications, the solution still describes the following main kinetics. (1) A thermal activation barrier hinders the transition at low temperatures. (2) Some overstepping (i.e. movement from the equilibrium boundary into the eclogite stability field) is necessary for the transition to occur. (3) Initially, the reaction rate increases exponentially with time where after it slows down again near the completion of the reaction. The parameters A_{kin} and E_{kin}^* determine how the reaction rate depends on the ambient temperature. These parameters can be estimated using geological and geophysical observations. Peak temperatures in the pT paths of partly eclogitised rocks range from 450 to 800 °C ([Hacker, 1996](#); [Austrheim, 1998](#)), although the upper value is mainly observed in essentially dry rocks, an unlikely situation in subduction zones. We can estimate suitable combinations of A_{kin} and E_{kin}^* from a p - T condition for which the reaction occurs well within the eclogite stability field, so that the term between square brackets in Eq. (9) is essentially I . For all experiments, we choose $A_{\text{kin}} = 10^{-6} \text{ s}^{-1}$. Values for E_{kin}^* are given in [Table](#)

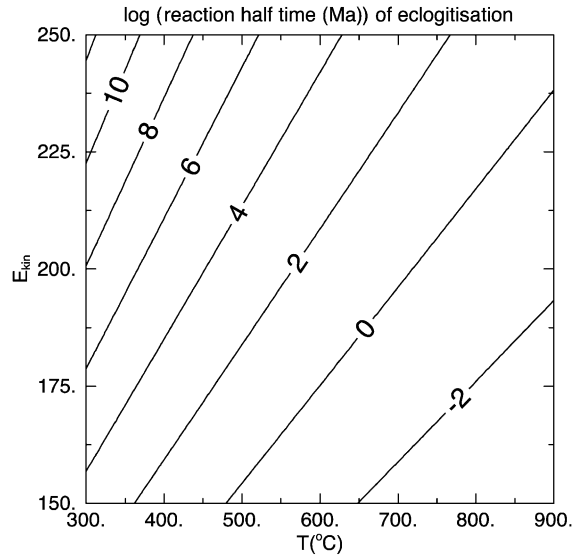


Fig. 2. Contourplot of the basalt-to-eclogite reaction rate as a function of given temperature T and kinetic activation energy E_{kin}^* . Contours give the logarithm of the reaction time to reach $\Gamma=0.5$ in Eq. (10).

3. The Gibbs free energy difference between the phases ΔG is calculated with parameters from [Putnis \(1992\)](#). [Fig. 2](#) shows the reaction half-time for the basalt-to-eclogite reaction as a function of ambient temperature T and kinetic activation energy E_{kin}^* by solving for $\Gamma=0.5$ in Eq. (10).

3. Results

3.1. Buoyancy effect of a subducting plateau

The capacity of an oceanic plateau to flatten a subducting slab is investigated through a series of model calculations. By variation of several model parameters, the robustness of the results were tested. In this section, we describe the influence of the most dominating parameters ([Table 3](#)). We defined the reference model REFp with an oceanic plateau and its equivalent without a plateau as model REFnp ([Tables 1–3](#)). The slab reaches a depth of 100 km at almost 500 km from the trench ([Fig. 3](#)). This large distance is due to the absence of a forebulge, which causes the slab to enter the trench with a zero dip angle. In model REFp, the subduction of the plateau causes a flat segment,

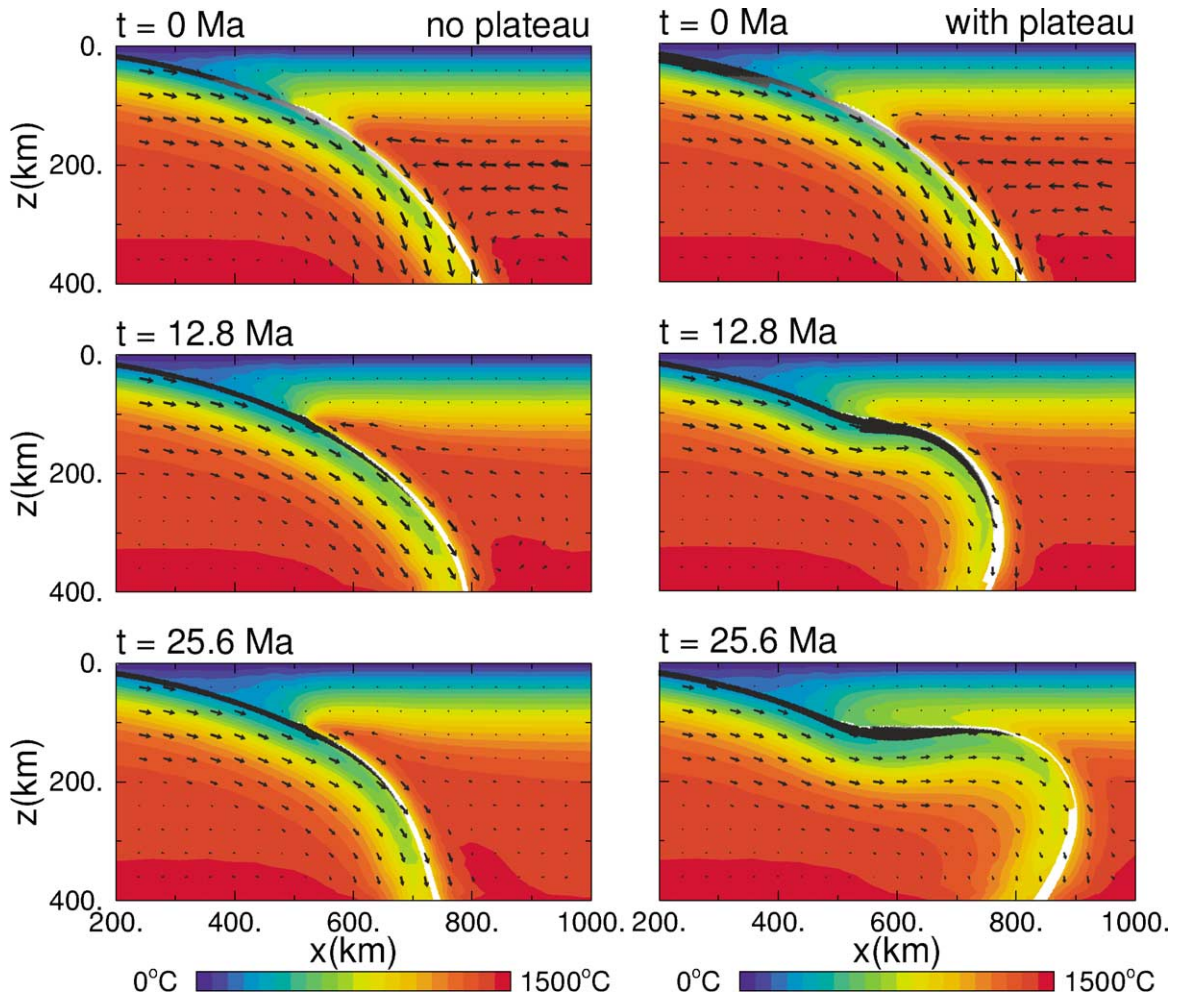


Fig. 3. Temperature contourplot (colors) of the subduction process in time for a subducting oceanic plateau (right, model REFp) in comparison with the subduction of 'normal' oceanic lithosphere (left, model REFnp). Black-and-white area represents the transition from basalt (black) to eclogite (white). Time increases from $t=0$ Ma at the beginning of the plateau subduction to the final stage of the plateau subduction at 25 Ma. Horizontal axis gives the distance to the trench, vertical axis the depth.

whereas model REFnp shows no flattening. The length of the flat-slab segment is a few hundred kilometers, measured from the position where the slab bends to the horizontal to the point where the slab steepens again to subduct further into the mantle. The thickened basaltic plateau crust and underlying thickened harzburgite layer provide enough buoyancy to support the slab, whereas a normal oceanic slab does not. Basalt transforms into eclogite as the slab warms up at its arrival in the hot asthenosphere. This process is initiated at the

top of the crust and later migrates to deeper parts of the crust, approximately along with the isotherms, as can be seen from the gradual thinning of the black crustal area in Fig. 3. After eclogitisation, the plateau becomes gravitationally unstable and causes further steep subduction or 'resubduction' into the mantle. Only during the horizontal subduction of the plateau, the length of the flat-slab segment increases. After resubduction of the plateau, the length of the flat slab remains approximately constant in time.

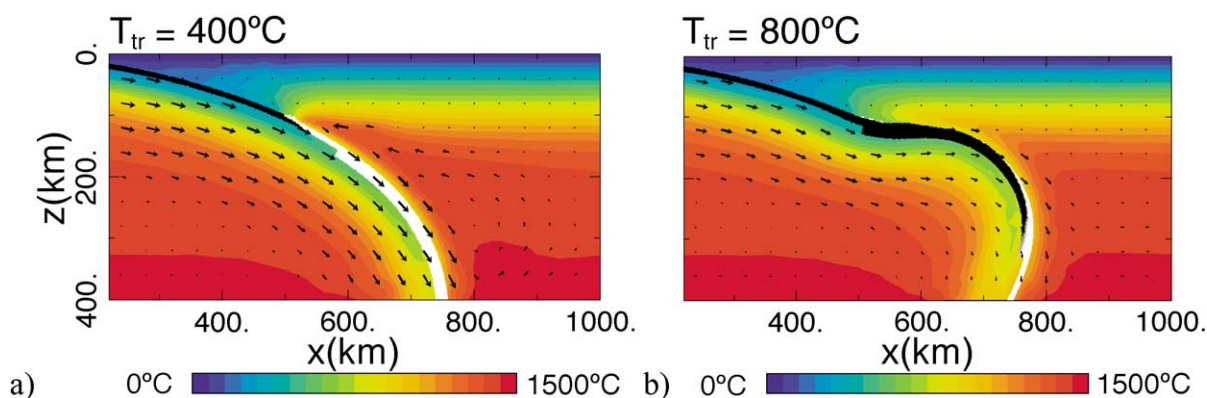


Fig. 4. Temperature contourplot of the plateau subduction process at $t=12.8$ Ma after initiation of plateau subduction. (a) With a transition temperature $T_{tr}=400$ °C, the compositional buoyancy is removed before flattening can start. (b) With $T_{tr}=800$ °C, the compositional buoyancy of the plateau flattens the slab.

3.2. Parameter sensitivity

3.2.1. Influence of the eclogitisation kinetics

The influence of the basalt-to-eclogite transformation rate on the dynamics of the subducting oceanic plateau is examined through variation of the activation energy E_{kin}^* in models REFp and KIN1 to KIN4. We varied E_{kin}^* between 146, 169, 192, 214 and 238 kJ/mol. At these values, 50% of the reaction takes place within the transition time $t_{tr}=10$ Ma at the temperatures of 400, 500, 600, 700 and 800 °C, respectively (see Fig. 2). We define this temperature to be the transition temperature T_{tr} . The transition time t_{tr} is chosen to represent a geologically significant time for the basalt to survive in a metastable phase. Fig. 4 shows the resulting slab dynamics at time $t=12.8$ Ma in case of plateau subduction for both extreme cases. The high T_{tr} case shows much similarity with the reference model results, shown in Fig. 3. The low T_{tr} case, however, shows no sign of flat subduction, eclogite is formed throughout the whole plateau almost with the first asthenospheric contact and the slab loses its compositional buoyancy before being able to flatten. In Fig. 5, the pressure–temperature–time paths (pTt paths) are shown for models KIN1 (with $T_{tr}=400$ °C) and model REFp (with $T_{tr}=700$ °C) for two monitor points, advected in the subducting slab. These points are positioned at the leading and trailing edge of the subducting plateau, 10 km below the surface of the slab. In model KIN1, the plateau has little influence on the subduction geometry:

the leading edge and later the trailing edge of the plateau describe a rather similar pT path. In model REFp, however, the slab flattens during the plateau subduction: the leading edge still subducts relatively steeply, but the trailing edge already subducts horizontally below the continent, at about 4-GPa pressure. The slab heats up and eclogitisation becomes significant above $T=700$ °C. Finally, pressure increases

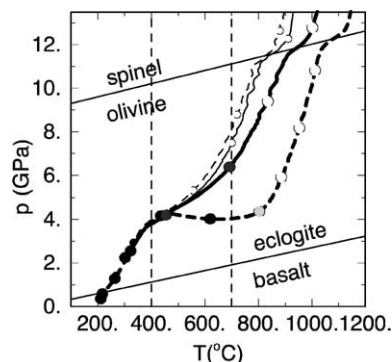


Fig. 5. Pressure–temperature–time (pTt) paths of the subduction process for model REFp ($T_{tr}=700$ °C, thick lines) and KIN1 ($T_{tr}=400$ °C, thin lines). Each path represents a point which was located 10 km below the surface before subduction (about halfway the basaltic unit of the plateau). Solid and dashed lines represent points on the leading and trailing edge of the plateau, respectively. Symbols are plotted every 3.2 Ma and represent the eclogitisation from basalt (black) to eclogite (white). Diagonal lines give the equilibrium position of the basalt-to-eclogite and olivine-to-spinel transitions. Vertical dashed lines show T_{tr} for models KIN1 and REFp at 400 and 700 °C, respectively.

again as the slab ‘resubducts’ further into the mantle. Fig. 6a shows the development in time of the flat-slab segment due to plateau subduction for several transition temperatures T_{tr} . Flattening of the plateau only occurs if basalt is able to survive a temperature of at least 700 °C. The results show a bimodal distribution in the style of subduction and the transition between steep and flat slabs is remarkably sharp: a flat slab either develops completely or not at all.

3.2.2. Influence of the slab strength

The low temperature of the slab interior results in large resistance against deformation by diffusion

creep or dislocation creep. Near the surface, brittle failure limits the strength of lithospheric plates, but at larger depth this mechanism is not effective. To avoid an unrealistically large strength of the subducting slab, an additional yield stress deformation mechanism is applied (see, e.g. (Ranalli, 1987; Kohlstedt et al., 1995)). Section 2.1 describes the implementation of this mechanism. This temperature-independent stress-limiting creep mechanism governs the deformation of the slabs, which is consistent with the idea that plate velocities are relatively insensitive to changes in the mantle temperature (Conrad and Hager, 1999). For the reference model REFp, this yield stress τ_y was quite

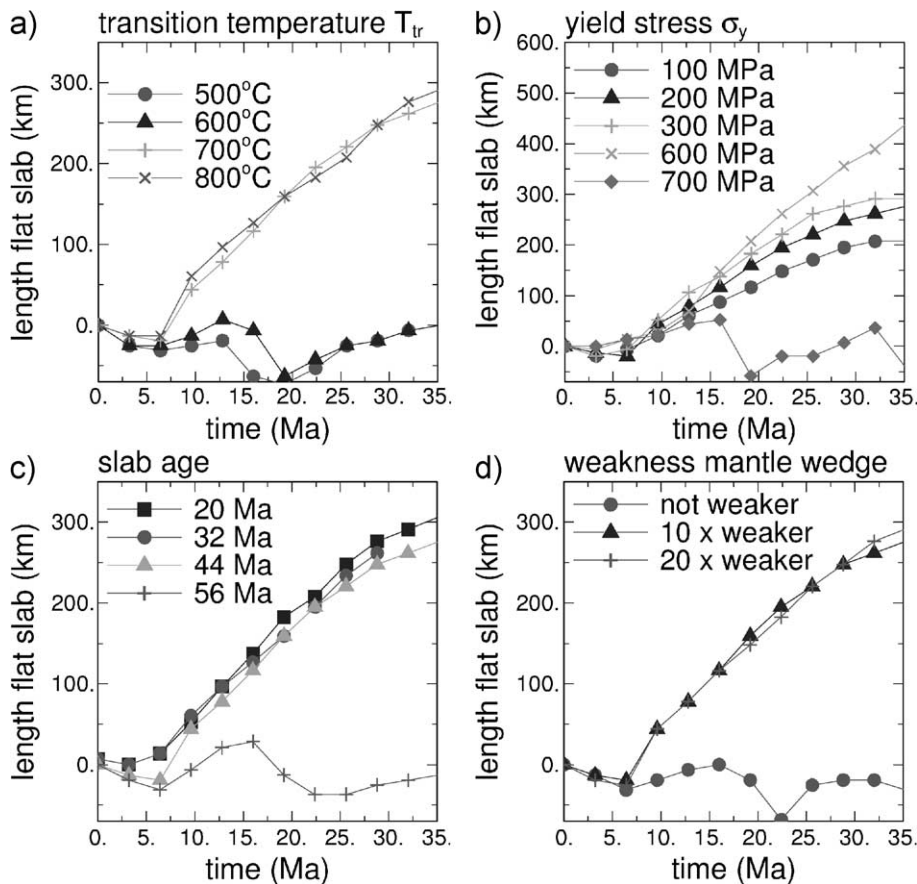


Fig. 6. Length of the flat slab segment in time for different values of the most critical model parameters. (a) Transition temperature, T_{tr} . $T_{tr} \leq 600$ °C gives steep plateau subduction, $T_{tr} \geq 600$ °C gives a flat subducting plateau. (b) Yield stress, τ_y . For $\tau_y \leq 600$ MPa, a larger slab strength resists immediate bending after eclogitisation more strongly than a weak one. For $\tau_y > 600$ MPa, the slab is too strong to bend to the horizontal and steep subduction is continued. (c) Slab age at the trench. Only slabs of 44 Ma old or younger are sufficiently buoyant to be supported by the oceanic plateau. (d) Relative strength of the mantle wedge and lowermost overriding continent. A mantle wedge weakening of one order of magnitude is required to allow a change in the style of subduction.

arbitrarily chosen to be 200 MPa. In models REFp and YLD1 to YLD9, the importance of this yield stress was evaluated by varying it between 100 MPa and 1 GPa. Fig. 6b combines these results. Up to $\tau_y = 600$ MPa, an increase in the yield stress results in an increased flat slab length: during its horizontal motion, the slab slowly loses its compositional buoyancy due to ongoing eclogitisation, until a point is reached where the slab is dense enough to continue its descent into the mantle. From that point on, the mechanical coherence of the slab mainly determines the dip angle. A weak slab allows immediate resubduction, while a strong slab will resist bending and descending. For $\tau_y > 600$ MPa, the slab is so strong, that even the initial bending phase of the buoyant plateau towards the horizontal is not possible: the available buoyancy force is smaller than the necessary force to bend the slab. In that case, the slab continues its initial descent at the trench and no flat-slab segment is created at all. In addition to this set of experiments, we performed several calculations to investigate the combined effects of the maximum yield strength of the material and the transition temperature of the basalt-to-eclogite transition. The clear distinction between flat and steep subducting slabs suggests the possibility of a different representation of the results, as shown in Fig. 7. An increasing slab strength requires only a slightly increasing transition temperature T_{tr} , up to which basalt remains metastable: the minimum required T_{tr} is about 600–700 °C, and depends only weakly on the slab strength.

If a buoyant oceanic plateau is the dominant mechanism for the creation of shallow flat subduction, these results have implications for the maximum strength of subducting slabs. On the one hand, model calculations with $\tau_y < 100$ MPa showed too little rigidity for the development of a large flat-slab segment. In this case, the dip angle of the slab has very little significance, since plate-like behavior is almost absent. On the other hand, flat subduction with $\tau_y \geq 600$ MPa required basalt metastability to an unrealistically high temperature of 800 °C. Thus, the maximum slab strength that allows for flat subduction is only about one order of magnitude higher than the minimum strength to maintain mechanical rigidity, and the reasonable range for the maximum slab strength is rather limited. The existence of flat subduction, therefore, may indicate that slabs are some, but not many orders of magnitude

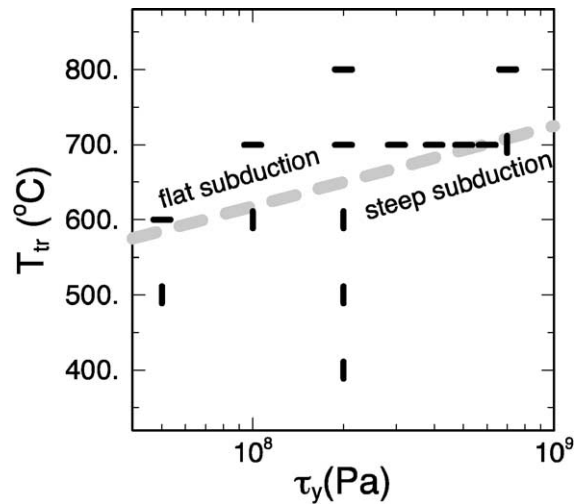


Fig. 7. Subduction dynamics for various maximum yield stresses τ_y and eclogitisation transition temperatures T_{tr} . Flat subduction is indicated with a horizontal line, steep subduction with a vertical line. The grey dashed line indicates the approximate transition between steep and flat subduction. Except for very weak slabs, flat subduction requires $T_{tr} = 700$ °C and $\tau_y > 600$ MPa requires an even higher T_{tr} .

stronger than the surrounding mantle material. This inference is in agreement with the conclusion of Moresi and Gurnis (1996), who favor weak slabs that cannot act as stress guides from the deep mantle to the surface. Based on similar criteria, Houseman and Gubbins (1997) suggest from numerical model simulations on slab deformation that only a narrow transition between too strong and too weak slabs can explain the slab geometry and stress orientation of the Tonga subduction zone, and that a slab is approximately 200 times more viscous than the upper mantle. Conrad and Hager (2001) showed that plates and slabs should be sufficiently viscous (10^{23} Pa s), but their total strength should be limited to produce plate-like surface motions. These results all suggest that a suitable range for the maximum strength of the slab is quite limited, and reasonably well constrained.

3.2.3. Influence of the age of the slab

Variation of the age of the subducting plate has an effect which is comparable to the variation of the slab strength in the former subsection. Results of models REFp and AGE1 to AGE3 are plotted in Fig. 6c. The age of the subducting plate at the trench ranges from 20

to 56 Ma. For all slabs of 44 Ma or younger, the plateau is able to produce a flat-slab segment. The 56-Ma old slab, however, fails to bend to the horizontal and continues its descent into the mantle. Again, the strength of the slab plays an important role, since older slabs are colder and mechanically stronger than young slabs. Another effect of the age variation comes from the thermal buoyancy: the old and cold slab is denser than a young, warm slab and, hence, has a larger negative thermal buoyancy. By comparing thermal and compositional buoyancy forces, Cloos (1993) calculated that an oceanic plateau with a 17-km thick crust is neutrally buoyant at the age of approximately 80 Ma, when the lithosphere is about 100 km thick. Gutscher et al. (2000) suggested that an 18-km thick crustal oceanic plateau is sufficiently buoyant to support itself, including an adjacent portion of normal slab with comparable width for lithospheric ages up to 50 Ma. We compared thermal and compositional buoyancy of the slab using an analytical cooling half-space approach. The extra mass per unit area of the oceanic lithosphere due to thermal contraction Δm_T is calculated (Turcotte and Schubert, 1982, Chap. 4, paragraph 22):

$$\Delta m_T = 2\alpha\rho_m T_m \sqrt{\frac{\kappa t}{\pi}} \quad (12)$$

Compositional buoyancy is calculated using relative density values of -400 and -77 kg/m^3 for basalt/gabbro and harzburgite, respectively. Fig. 8 shows the total (thermal and compositional) buoyancy for different crustal thicknesses before eclogitisation. Normal oceanic crust has a thickness of about 7 km and becomes gravitationally unstable at 25 Ma, but a thicker crust is also stable at greater age. According to this estimate and the ones by Cloos (1993) and Gutscher et al. (2000), a plateau with an 18-km thick crust will be buoyant even for the oldest oceanic lithospheres found on Earth today. The absence of a flat plateau in the 56-Ma lithosphere model calculation from Fig. 6c is not in agreement with these estimates for two reasons. First, the total integrated buoyancy of the slab may be smaller than predicted from the 1-D model on which Eq. (12) is based: parts of the slab around the plateau have no thickened crust and the plateau should be able to support those parts as well; partial eclogitisation of the plateau may already neu-

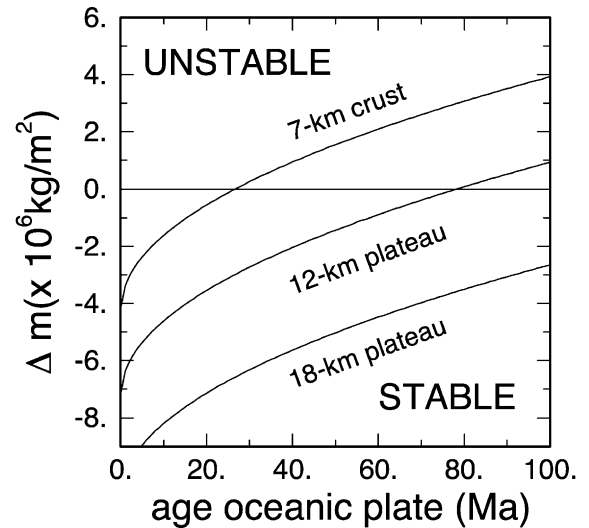


Fig. 8. Integrated buoyancy estimates of oceanic lithosphere before eclogitisation as a function of the age of the oceanic plate for crustal thicknesses of 7, 12 and 18 km. Normal oceanic lithosphere (7-km crust) remains buoyant until an age of ~ 25 Ma, while a plateau with an 18-km crust remains buoyant even at high ages.

tralize some of the compositional buoyancy in an early stage in the subduction process. Second, the analytical buoyancy calculations do not take into account the forces that are required to bend the slab. Section 3.2.2 shows that we cannot discard the strength of the slab.

3.2.4. Mantle wedge deformation due to the changing subduction style

To allow a change from steep to shallow horizontal subduction, the lowermost part of the lithosphere and the mantle wedge should be able to deform to adapt to the new subduction style. During continuous steep subduction prior to the plateau subduction, the overlying continent and mantle wedge are cooled by thermal conduction in the vicinity of the slab. When the deformation laws for dry mantle material are applied in the mantle wedge, a vertical extension of the strong overlying lithosphere is formed in the mantle wedge corner, as shown in Fig. 9. This prohibits a shallow change in the dip angle. A more realistic rheology description, however, may include hydrous weakening of the overlying mantle wedge as a result of dehydration of the underlying slab (Tatsumi and Eggins, 1995; Karato, submitted for publication), as this process continuously delivers water to the mantle

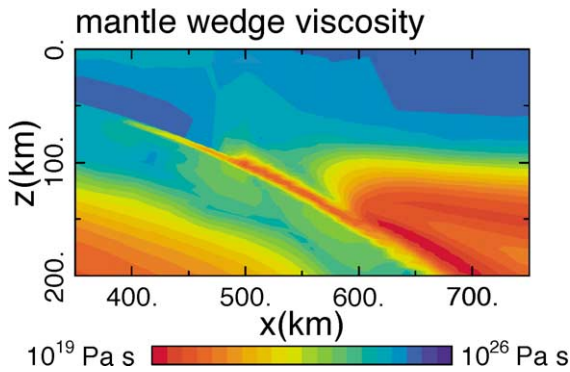


Fig. 9. Continuous cooling in the vicinity of the steeply subducting slab may result in a vertical extension of the strong overlying continental lithosphere in the mantle wedge corner, in case no hydrous weakening is applied in this region.

wedge. We investigated the effect of hydrous mantle wedge weakening on the dynamics of the subducting plateau using models REFp, WMW1 and WMW2. To model the effect of hydrous weakening, we applied a regional weakening in a 150-km wide zone in the mantle wedge corner above the slab and below the depth of 100 km. We applied a weakening relative to the dry mantle material, using a local change in the viscosity prefactor $A_{k,m}$ ranging from 1 (no weakening) to 0.05 ($20 \times$ weaker mantle wedge). Model REFp contains an intermediate weakening of 0.1 ($10 \times$ weaker mantle wedge). Fig. 6d combines the results of the various amounts of weakening in terms of a resulting length of the flat slab region as a function of time. The model without a weakened mantle wedge does not show any development of a flat-slab segment, while a weakening of one order of magnitude is sufficient to allow the necessary mantle wedge deformation for the flattening. A further decrease of the mantle wedge strength does not further change the slab geometry. For further elaboration of the effects of a weak mantle wedge, we refer to Billen and Gurnis (2001).

4. Discussion

4.1. The limited lateral extent of the plateau along the trench

All model results were obtained with a two-dimensional subduction model. Strictly speaking, such

model only applies to a subduction process without any changes in the direction along-trench. Aseismic ridges and especially seamount chains are long and relatively narrow features, for which this 2-D model may not apply. Even flat-subducting oceanic plateaus only form a small portion of the total subducting plate at the trench. The possible transition between the flat-subducting plateau and neighboring steep-subducting normal oceanic lithosphere is illustrated by Sacks (1983) and Gutscher et al. (1999) and is described by either a gradual change in the subduction dip angle or an abrupt one, in case the slab tears. If the slab does not tear, we expect an extra slab pull force on the sides of the subducting plateau, so that the horizontal subduction is hindered by a larger total slab pull. In that case, the presented model results probably form an upperbound on the ability of such a plateau to support the slab.

4.2. The transition between steep and flat subducting plateaus

Examination of time series plots in Fig. 6 reveals a bimodal behavior because it shows that a flat-slab segment is either fully created or not at all, and that an intermediate-angle subduction regime does not occur. Apparently, initial flattening of the slab strengthens the ability to flatten the slab even more. Several mechanisms could be responsible for this feature. On the one hand, the heating of the top of the slab is retarded if the slab subducts horizontally, since it is not in contact with hot asthenosphere in the mantle wedge, but with the much cooler base of the continent. This results in a delay of the basalt-to-eclogite transition, which keeps the slab buoyant further away from the trench. It also delays the thermal weakening of the slab, so that it does not immediately resubduct after eclogitisation. However, in our models a significant delay in the heating and eclogitisation of a flat slab is not observed as compared to steeper subduction (Fig. 3). On the other hand, the dynamic pressure from the mantle wedge flow exerts a torque on the slab that tends to decrease the subduction dip angle. This mechanism was already proposed by Tovish et al. (1978). They showed that this effect increases with decreasing dip angle, as the mantle wedge is getting narrower, and suggested this to be a mechanism to explain the gap in observed subduction angles between about 10° and

20°. In addition, we expect a contribution from the viscous coupling between the converging plates. This resisting force forms another torque in combination with the forced subduction of the buoyant plateau by the rest of the gravitationally unstable plate. The origin of both torques is similar: both result from the combination of resistance at the top of the slab and a driving force in the direction of the slab motion. All mechanisms, proposed in this subsection, are implicitly incorporated in the numerical model. It is, therefore, difficult to distill the significance of each of these effects separately.

4.3. Evolution after plateau subduction

Since most slabs subduct rather steeply and flat subduction occurs only at about 10% of the convergent zones (Gutscher et al., 2000), we expect this geometry to be a transient phenomenon, for the duration of the plateau subduction, and to disappear afterwards. In our model results, however, the flat slab becomes a permanent feature, once it is initiated by the plateau subduction. Apparently, flat subduction is a stable feature in our model setup, and only needs to be triggered by the plateau subduction. In the previous section, we discussed mechanisms for the absence of subduction with a dip angle between 10° and 20°. These mechanisms could also be responsible for the absence of the ‘resteeptening’ of the slab, as they offer a preference for the slab to stick to the overlying continent. Yet another explanation could come from the two-dimensionality of the model: inflow of asthenospheric mantle material is necessary to separate the slab from the overriding continent again. In a 2-D model, this flow can only come from the ‘inland’ direction perpendicular to the trench. In a 3-D model, this asthenospheric inflow is also possible along-trench from an area of steeper subduction, where a mantle wedge still separates the subducting and overlying plates.

4.4. Other mechanisms and shallow flat slab observations

For the subduction zone at the Nankai Trough near Japan, a flat slab is present at a distance of at least 200 km from the trench (Sacks, 1983; Gutscher et al., 2000). Direct comparison with the maximum distance

between trench and the modeled flat slab is not possible due to the absence of a forebulge in our model, which overestimates the horizontal extent of the ‘forearc.’ Therefore, we prefer to compare the observed length of the actual flat-slab segment with the one from our model calculations. Subtracting the initial steeper part of the subduction zone from the trench to a depth of about 100 km, leaves a flat slab length of approximately 100 km below Japan. Our model results suggest that this agrees well with our model results. Below Peru and Central Chile, however, a flat slab is observed more than 700 km from the trench (Gutscher et al., 2000). Subtracting again the part at which the slab subducts from the surface to a depth of 100 km depth, results in an actual flat-slab segment of about 400–500 km length. The model calculations generally do not show a flat slab of such length. The results displayed in Fig. 6 mostly show a maximum flat slab length between 200 and 300 km. As discussed above, this length should be regarded as an upperbound in case of a continuous lateral slab across the edge of the plateau. The dynamical pressure effect as discussed by Tovish et al. (1978) is implicitly included in our viscous flow model. The spatial and temporal correlation between the subducting oceanic Nazca Ridge and Juan Fernandez Ridge and the occurrence of the Peru and Central Chile flat slab regions, respectively, strongly suggest a causal relation, but the buoyancy and strength of a subducting oceanic plateau seem to be insufficient to explain the observed flat slab extent of 400–500 km. Lithospheric doubling has been proposed as an alternative mechanism to explain shallow flat subduction (Vlaar, 1983; van Hunen et al., 2000). In this mechanism, an active trenchward motion of the overriding continent is responsible for the flattening of a slab. Indeed, the continent of South America has a westward absolute motion of about 3 cm/year with respect to the hotspot reference frame (Olbertz et al., 1997; Olbertz, 1997). The combined effects of the subducting plateau and the trenchward overriding plate motion is probably most successful in explaining the flat subduction below Peru and Central Chile. The numerical results from this study confirm to a large extent the qualitative conclusions, based on observations from Cross and Pilger (1982) that the subduction dip angle is determined by the combined effects from the absolute (trenchward) overriding plate motion, convergence

rate, the presence of subducting seamounts, aseismic ridges or oceanic plateaus and finally by the age of the subducting plate (see also Vlaar and Wortel, 1976).

The formation of the Rocky Mountains during the Sevier–Laramide orogeny has been attributed to flat subduction (Dickinson and Snyder, 1978), with a maximum flat-slab segment as long as 1500 km approximately 65 Ma ago. The presented model results show that the subduction of an oceanic plateau is not capable of the creation of a flat-slab segment of this extent. Besides, the distribution of igneous activity from 60 to 35 Ma (Dickinson and Snyder, 1978) shows a continuous and much larger north–south extending flat subduction event than is the case for the flat subduction below South America today. Although the buoyancy of subducting plateaus can certainly have contributed, the proposed westward motion of North America of about 5 cm/year from 60 to 45 Ma (Engelbreton et al., 1985) suggest that active overthrusting was the dominant mechanism of the Laramide shallow flat subduction.

5. Conclusion

As an attempt to explain the occurrence of flat subduction at approximately 10% of the Earth's subduction zones, the subduction of buoyant oceanic plateaus has been proposed as a possible mechanism. We applied a two-dimensional finite element model to examine the physical circumstances for which a subducting oceanic plateau causes shallow flat subduction. We performed a series of model calculations to determine the most influencing physical model parameters in this process. The most important criterion for the occurrence of a flat-subducting plateau is the presence of metastable basalt in the eclogite stability field. Model calculations on a 44-Ma subducting slab demonstrate that basalt should be able to survive a temperature of at least 600–700 °C to keep the plateau buoyant sufficiently long to cause a flat-slab segment. These models further showed that yield stresses in the slab should not exceed 600 MPa to allow for the necessary bending of the slab to change its dip. Furthermore, the strength of the bottom of the continent and the mantle wedge is a critical factor in the development of a flat-slab segment, and our simulations suggest

that hydrous weakening of this region above the slab should be at least one order of magnitude to allow for the deformation that is required to change the style of subduction.

In most model calculations, the length of an occurring flat-slab segment was limited to about 300 km. The limited metastability of the oceanic basaltic crust and the decreasing strength of the slab during its journey through the mantle do not allow for further horizontal movement. This is likely to be sufficient for the flat-slab occurrence at the Nankai Trough, but addition of another mechanism, like active overthrusting of the continental plate, is necessary to explain a flat-slab segment as far as 700 km from the trench, as proposed below Peru or Central Chile today, or an even larger flat slab region of about 1500 km below the western USA around 65 Ma ago.

Acknowledgements

The authors would like to thank Bertram Schott, Michel Jacobs, Herman van Roermund, Timm John and Rob van der Hilst for helpful discussions, and David Yuen and Greg Houseman for constructive reviews. This work was sponsored by the Stichting Nationale Computerfaciliteiten (National Computing Facilities Foundation, NCF) for the use of super-computer facilities, with financial support from the Nederlandse Organisatie voor Wetenschappelijk Onderzoek (Netherlands Organization for Scientific Research, NWO).

References

- Abers, G.A., 2000. Hydrated subducted crust at 100–250 km depth. *Earth Planet. Sci. Lett.* 176, 323–330.
- Ahrens, T.J., Schubert, G., 1975. Gabbro–eclogite reaction rate and its geophysical significance. *Rev. Geophys. Space Phys.* 13 (2), 383–400.
- Austrheim, H., 1998. Influence of fluid and deformation on metamorphism of the deep crust and consequences for the geodynamics of collision zones. In: Hacker, B., Liou, J. (Eds.), *When Continents Collide: Geodynamics and Geochemistry of Ultra-high-Pressure Rocks*. Kluwer Academic Publishers, Dordrecht, pp. 297–323.
- Billen, M.I., Gurnis, M., 2001. A low viscosity wedge in subduction zones. *Earth Planet. Sci. Lett.* 193, 227–236.
- Bird, P., 1988. Formation of the rocky mountains, Western United States: a continuum computer model. *Science* 239, 1501–1507.

- Chapman, D.S., 1986. Thermal gradients in the continental crust. In: Dawson, J.B., Carswell, D.A., Hall, J., Wedepohl, K.H. (Eds.), *The Nature of the Lower Continental Crust*. Geological Society, Spec. Publ. No. 24, pp. 63–70.
- Cloos, M., 1993. Lithospheric buoyancy and collisional orogenesis: subduction of oceanic plateaus, continental margins, island arcs, spreading ridges, and seamounts. *Geol. Soc. Amer. Bull.* 105, 715–737.
- Conrad, C.P., Hager, B.H., 1999. The thermal evolution of an earth with strong subduction zones. *Geophys. Res. Lett.* 26 (19), 3041–3044.
- Conrad, C.P., Hager, B.H., 2001. Mantle convection with strong subduction zones. *Geophys. J. Int.* 144, 271–288.
- Cross, T.A., Pilger Jr., R.H. 1982. Controls of subduction geometry, location of magmatic arcs, and tectonics of arc and back-arc regions. *Geol. Soc. Amer. Bull.* 93, 545–562.
- Däßler, R., Yuen, D., Karato, S.-I., Riedel, M., 1996. Two-dimensional thermo-kinetic model for the olivine–spinel phase transition in subducting slabs. *Phys. Earth Planet. Inter.* 94, 217–239.
- Dickinson, W., Snyder, W., 1978. Plate tectonics of the Laramide orogeny. *Geol. Soc. Am. Mem.* 151, 355–366.
- Engelbreton, D.C., Cox, A., Gordon, R.G., 1985. Relative motions between oceanic and continental plates in the Pacific basin. *Geol. Soc. Am., Spec. Pap.* 286, 1–59.
- Giunchi, C., Ricard, Y., 1999. High-pressure/low-temperature metamorphism and the dynamics of an accretionary wedge. *Geophys. J. Int.* 136, 620–628.
- Gubbins, D., Snieder, R., 1991. Dispersion of P waves in subducted lithosphere: evidence for an eclogite layer. *J. Geophys. Res.* 96 (B4), 6321–6333.
- Gutscher, M.-A., Olivet, J.-L., Aslanian, D., Eissen, J.-P., Maury, R., 1999. The “lost Inca Plateau”: cause of flat subduction beneath Peru? *Earth Planet. Sci. Lett.* 171, 335–341.
- Gutscher, M.-A., Spakman, W., Bijwaard, H., Engdahl, E., 2000. Geodynamics of flat subduction: seismicity and tomographic constraints from the Andean margin. *Tectonics* 19 (5), 814–833.
- Hacker, B.R., 1996. Eclogite formation and the rheology, buoyancy, seismicity and H₂O content of oceanic crust. *Subduction: Top to Bottom*. American Geophysical Union, Monogr. No. 96, 337–346.
- Hacker, B.R., Bohlen, S.R., Kirby, S.H., 1993. Albite → jadeite + quartz transformation in albitite. *Eos, Trans. - Am. Geophys. Union* 74, 611.
- Holland, T.J.B., 1980. The reaction albite = jadeite + quartz determined experimentally in the range 600–1200 °C. *Am. Mineral.* 65, 129–134.
- Houseman, G.A., Gubbins, D., 1997. Deformation of subducted oceanic lithosphere. *Geophys. J. Int.* 131, 535–551.
- Irifune, T., Ringwood, A.E., 1993. Phase transformations in subducted oceanic crust and buoyancy relations at depths of 600–800 km in the mantle. *Earth Planet. Sci. Lett.* 117, 101–110.
- Ita, J., King, S.D., 1994. Sensitivity of convection with an endothermic phase change to the form of governing equations, initial conditions, boundary conditions, and equation of state. *J. Geophys. Res.* 99 (B8), 15919–15938.
- Jarrard, R.D., 1986. Relations among subduction parameters. *Rev. Geophys.* 24 (2), 217–284.
- Jischke, M.C., 1975. On the dynamics of descending lithospheric plates and slip zones. *J. Geophys. Res.* 80 (35), 4809–4813.
- Kameyama, M., Yuen, D.A., Karato, S.-I., 1999. Thermal–mechanical effects of low-temperature plasticity (the Peierls mechanism) on the deformation of a viscoelastic shear zone. *Earth Planet. Sci. Lett.* 168, 159–172.
- Karato, S.-I., 2001. Mapping water content in the upper mantle. *Subduction Factory*. American Geophysical Union, Monogr., in press.
- Karato, S.-I., Jung, H., 2001. Effects of pressure on high-temperature dislocation creep in olivine. *Philos. Mag.*, A., in press.
- Karato, S.-I., Rubie, D.C., 1997. Toward an experimental study of deep mantle rheology: a new multianvil sample assembly for deformation studies under high pressures and temperatures. *J. Geophys. Res.* 102 (B9), 20122–21111.
- Karato, S.-I., Wu, P., 1993. Rheology of the upper mantle: a synthesis. *Science* 260, 771–778.
- Kirby, S., Engdahl, E.R., Denlinger, R., 1996a. Intermediate-depth intraslab earthquakes and arc volcanism as physical expressions of crustal and uppermost mantle metamorphism in subducting slabs. *Subduction: Top to Bottom*. American Geophysical Union, Monogr. No. 96, 195–214.
- Kirby, S.H., Stein, S., Okal, E.A., Rubie, D.C., 1996b. Metastable mantle phase transformations and deep earthquakes in subducting oceanic lithosphere. *Rev. Geophys.* 34 (2), 261–306.
- Kirkpatrick, R., 1976. Towards a kinetic model for the crystallization of a magma body. *J. Geophys. Res.* 81, 2565–2571.
- Kohlstedt, D.L., Evans, B., Mackwell, S.J., 1995. Strength of the lithosphere: constraints imposed by laboratory experiments. *J. Geophys. Res.* 100 (B9), 17587–17602.
- McGeary, S., Nur, A., Ben-Avraham, Z., 1985. Spatial gaps in arc volcanism: the effect of collision or subduction of oceanic plateaus. *Tectonophysics* 119, 195–221.
- Mei, S., Kohlstedt, D.L., 2000a. Influence of water on plastic deformation of olivine aggregates: 1. Diffusion creep regime. *J. Geophys. Res.* 105, 21457–21469.
- Mei, S., Kohlstedt, D.L., 2000b. Influence of water on plastic deformation of olivine aggregates: 2. Dislocation creep regime. *J. Geophys. Res.* 105, 21471–21481.
- Moresi, L., Gurnis, M., 1996. Constraints on the lateral strength of slabs from three-dimensional dynamic flow models. *Earth Planet. Sci. Lett.* 138, 15–28.
- Olbertz, D., 1997. The long-term evolution of subduction zones: a modelling study. PhD thesis, Utrecht University, The Netherlands.
- Olbertz, D., Wortel, M.J.R., Hansen, U., 1997. Trench migration and subduction zone geometry. *Geophys. Res. Lett.* 24, 221–224.
- Putnis, A., 1992. *Introduction to Mineral Sciences* Cambridge Univ. Press.
- Ranalli, G., 1987. *Rheology of the Earth, Deformation and Flow Processes in Geophysics and Geodynamics* Allen & Unwin, Boston, MA.
- Riedel, M.R., Karato, S.-I., 1996. Microstructural development during nucleation and growth. *Geophys. J. Int.* 125, 397–414.
- Rubie, D., 1990. Role of kinetics in the formation and preservation

- of eclogites. In: Carswell (Ed.), *Eclogite Facies Rocks*. Blackie, Glasgow, pp. 111–140.
- Sacks, I.S., 1983. The subduction of young lithosphere. *J. Geophys. Res.* 88 (B4), 3355–3366.
- Saunders, A., Tarney, J., Kerr, A., Kent, R., 1996. The formation and fate of large oceanic igneous provinces. *Lithos* 37, 81–95.
- Schmeling, H., Monz, R., Rubie, D.C., 1999. The influence of olivine metastability on the dynamics of subduction. *Earth Planet. Sci. Lett.* 165, 55–66.
- Shelton, G., Tullis, J., 1981. Experimental flow laws for crustal rocks. *Eos, Trans. - Am. Geophys. Union* 62 (17), 396.
- Steinbach, V., Hansen, U., Ebel, A., 1989. Compressible convection in the Earth's mantle—a comparison of different approaches. *Geophys. Res. Lett.* 16 (7), 633–636.
- Stevenson, D.J., Turner, S.J., 1977. Angle of subduction. *Nature* 270, 334–336.
- Tatsumi, Y., Eggins, S., 1995. *Subduction Zone Magmatism*. Blackwell, Oxford.
- Tovish, A., Schubert, G., Luyendyk, B.P., 1978. Mantle flow pressure and the angle of subduction: non-Newtonian corner flows. *J. Geophys. Res.* 83 (B12), 5892–5898.
- Turcotte, D.L., Schubert, G., 1982. *Geodynamics, Applications of Continuum Physics to Geological Problems*. Wiley, New York, NY.
- van den Berg, A.P., van Keken, P.E., Yuen, D.A., 1993. The effects of a composite non-Newtonian and Newtonian rheology on mantle convection. *Geophys. J. Int.* 115, 62–78.
- van Hunen, J., van den Berg, A.P., Vlaar, N.J., 2000. A thermo-mechanical model of horizontal subduction below an overriding plate. *Earth Planet. Sci. Lett.* 182, 157–169.
- van Hunen, J., van den Berg, A.P., Vlaar, N.J., 2001. Latent heat effects of the major mantle phase transitions on low-angle subduction. *Earth Planet. Sci. Lett.* 190, 125–135.
- Vlaar, N.J., 1983. Thermal anomalies and magmatism due to lithospheric doubling and shifting. *Earth Planet. Sci. Lett.* 65, 322.
- Vlaar, N.J., Wortel, M.J.R., 1976. Lithospheric aging, instability and subduction. *Tectonophysics* 32, 331.